BRØNSTED ACIDITY OF H-[Ga]-ZSM-5 ZEOLITES AS DETERMINED BY VARIABLE-TEMPERATURE IR SPECTROSCOPY

Ana Canaleta Safont*, Carlos Palomino Cabello, Carlos Otero Areán, Gemma Turnes Palomino*

Department of Chemistry, University of the Balearic Islands, 07122 Palma de Mallorca

Spain

*Corresponding authors:

e-mail address: aina.canaleta@uib.eu

e-mail address: g.turnes@uib.es

Abstract

Protonic gallosilicates H-[Ga]-ZSM-5 were synthesized, following a hydrothermal procedure, from gels having Si/Ga ratios of 25, 50 and 75. Likewise, for comparison, protonic zeolites H-[Al]-ZSM-5 having Si/Al ratios of 25 and 50 were also prepared. Brønsted acidity of the structural Si(OH)Ga groups in the gallosilicates was studied by means of IR spectroscopy at a variable temperature (VTIR) using CO and N_2 as probe molecules. This instrumental technique enables one simultaneous measurement of the bathochromic shift of the stretching O−H mode, $\Delta\upsilon_{(OH)}$, of the Brønsted acid group interacting (through hydrogen bonding) with the probe molecule and the corresponding standard enthalpy change, ΔH^{0}, in the adsorption process. The results obtained clearly showed that the gallosilicates are distinctively less acidic than the aluminosilicates, whichever acidity indicator is used: $\Delta\upsilon_{(OH)}$ either or ΔH^{0}. Nevertheless, no change of Brønsted acid strength was found when changing the Si/Ga ratio.

Keywords: *Adsorption enthalpy, Brønsted acidity, Gallosilicates, Variable Temperature Infrared Spectroscopy (VTIR), Zeolites.*

1. Introduction

Protonic zeolites have found vast application as solid acid catalysts in a wide range of technological processes. The Bronsted acidic character of zeolites stems from the presence of bridging Si(OH)Al hydroxyl groups. Isomorphous replacement of silicon by another tetrahedrally coordinated elements, such as boron, indium or gallium, in addition to aluminium, has been used to modify the acid strength of zeolites [1–3]. The substitution of silicon by other elements different from aluminium can also influence the pore size distribution and the crystal size of the material [4]. This ability of vary the acid and textural properties of the zeolites allows tuning its catalytic behaviour for a particular reaction.

Interest in gallium substituted zeolites started in 1990, when the UPO-BP (British Petroleum) introduced [Ga]-ZSM-5 as a catalyst in the Cyclar process, which produces aromatics from short chain hydrocarbons [5,6]. The increasing applications of BTX aromatics (benzene, toluene and xylene) as basic feedstocks for the production of a wide range of industrial chemicals (*i.e.* gasoline blending components, production of styrene, phenol, terephthalic acid, phthalic anhydride, and isophthalic acid), have led to a large increase in the demand for aromatics [7] and a growing interest in gallium substituted zeolites [7–11]. Moreover, Ga modified zeolites have also been proposed for other catalytic processes like co-pyrolysis of biomass, production of levulinic acid from carbohydrates, glycerol dehydration or hydrodesulfurization of organosulfur compounds, among others [12–15]. In all these processes, the catalytic activity and selectivity of the gallosilicate depends on the Ga distribution between framework and extra-framework positions [16–18] which has been reported to be strongly affected by the Si/Ga ratio and the method used for Ga incorporation [19–22].

Several instrumental techniques are currently used for determining the Brønsted acid strength of zeolites. Among them, microcalorimetry of an adsorbed base (such as ammonia or pyridine), temperature programmed desorption and solid state NMR and IR spectroscopy [23–25]. Among these, infrared spectroscopy of an adsorbed weak base is very frequently used, mainly on account of its simplicity. The hydrogen-bonded species formed when a weak base is adsorbed on a protonic zeolite can easily be monitored by IR spectroscopy, because hydrogen bonding brings about a characteristic bathochromic shift of the O–H stretching frequency of the zeolite hydroxyl groups. Brønsted acidity has

been frequently correlated with the magnitude of this bathochromic shift: the larger the bathochromic shift, the stronger the Brønsted acid site is [26,27]. However, some authors have pointed out some possible drawbacks of this simple method [28–31]. An alternative is the measurement of the enthalpy change, ΔH^0, involved in the hydrogen bonding interaction by means of variable-temperature infrared (VTIR) spectroscopy [31–33].

Aiming at studying their acidity, protonic [Ga]-ZSM-5 zeolites were synthesized, following a hydrothermal procedure, from gels having Si/Ga ratios of 25, 50 and 75. For comparison, protonic [Al]-ZSM-5 zeolites, having Si/Al ratios of 25 and 50, were also prepared. Brønsted acidity of the H-[Al]-ZSM-5 zeolites and the isostructural H-[Ga]-ZSM-5 samples was determined by means of variable-temperature IR (VTIR) spectroscopy [32–34] using CO and N_2 as probe molecules, which are two of the more frequently used probe molecules for IR spectroscopic characterization of Brønsted acid sites in zeolites.

2. Materials and methods

2.1. Synthesis of [Ga]-ZSM-5 zeolites

Three Na-[Ga]-ZSM-5 zeolite samples having nominal Si/Ga ratios of 25, 50 and 75 were prepared by hydrothermal synthesis, following a similar procedure to that described by Simmons et al. [35]. In a typical synthesis, aqueous solutions containing the appropriate amounts of sodium silicate (Fluka, 97%), gallium nitrate (Aldrich, 99.9%), and tetrapropylammonium bromide (Fluka, 98%) were prepared separately (the quantities used of each of them are given in Table S1 in the supplementary information). After mixing the three solutions, H_2SO_4 (Panreac, 96%) was added with stirring until the pH was 10. The resultant gels were placed inside autoclaves with Teflon lining and heated under autogeneous pressure for 7 days at 443 K; the resulting products were thoroughly washed with distilled water and allowed to dry in air.

2.2. Synthesis of [Al]-ZSM-5 zeolites

For the sake of comparison, two Na-[Al]-ZSM-5 zeolite samples having nominal Si/Al ratios of 25 and 50 were prepared by adapting a procedure reported in the literature [36]. Appropriate amounts of sodium silicate (Fluka, 97%), sodium aluminate (Fisher Scientific, 100%), and tetrapropylammonium bromide (Fluka, 98%) were dissolved separately in water. The resultant solution was acidified with H_2SO_4 (Panreac, 96%) until a pH of 10 to give a gel, which was placed inside a Teflon-lined autoclave and heated to

443 K for 7 days under autogeneous pressure. The resulting crystalline solids were thoroughly washed with distilled water and allowed to dry in air.

2.3. Preparation of the protonic forms

Thermal decomposition of the structure directing agent of both, gallium and aluminium, zeolites was achieved by calcination at 773 K for 5 hours, using at the end of the calcination period an oxygen flow to burn off residual coke. After calcination, the samples were exchanged with an aqueous 1M ammonium nitrate solution at room temperature during 24 hours to obtain the ammonium forms, which were then thermolyzed at 673 K (inside the IR cell) to yield the corresponding protonic forms H-[Ga]-ZSM-5 and H-[Al]-ZSM-5. Samples will be referred to by the notation H-[Ga]-ZSM-5(X) and H-[Al]-ZSM-5(X) where X denotes the corresponding Si/Ga (25, 50 and 75) and Si/Al (25 and 50) ratio, respectively.

2.4. Preliminary characterization

Powder X-ray diffraction data were collected to examine sample crystallinity and phase purity using CuKα radiation on a Siemens D5000 diffractometer. Particle morphology was analyzed by scanning electron microscopy using a Hitachi S-3400N microscope operated at 15 kV. To give insight into the coordination state of Ga^{3+} and Al^{3+} in the corresponding gallo- and aluminosilicates, ^{71}Ga and ^{27}Al spectra were obtained on a Bruker Avance III 600 spectrometer equipped with a solid state probe Bruker MAS BB/1H of 4 mm. The ^{71}Ga and ^{27}Al NMR spectra were recorded at frequency of 183.01 MHz with a MAS spinning rate of 8 kHz and at frequency of 156.37 MHz with a MAS spinning rate of 14 kHz, respectively. The chemical shifts were measured relative to a gallium nitrate aqueous solution (1M) for ^{71}Ga NMR spectra and to an aluminium nitrate aqueous solution (1M) for ^{27}Al NMR spectra.

2.5. Variable-temperature infrared spectroscopy

For VTIR spectroscopy, thin self-supported wafers of the samples were prepared and activated (outgassed) in a dynamic vacuum (residual pressure smaller than 10^{-4} mbar) at 673 K for 8 h inside an IR cell, described elsewhere [37], that allowed us to perform: (i) in situ sample activation, (ii) gas dosage, and (iii) variable-temperature IR (VTIR) spectroscopy of the adsorbed probe molecule while simultaneously recording temperature and equilibrium pressure. A platinum resistance thermometer (Tinsley) and a capacitance

pressure gauge (MKS, Baratron) were used for that purpose; the precision of the measurements was about ±2 K and ±2x10^{-2} mbar for temperature and pressure, respectively.

After thermal activation of the sample wafer, the cell was cooled with liquid nitrogen, and in order to optimize thermal contact between the sample wafer and the cool cell body, 0.2 mbar of helium was admitted into the sample compartment before the background spectrum was recorded. The cell was then dosed with carbon monoxide and closed, and Transmission FTIR spectra were recorded from 157 to 228 K. Simultaneously, the temperature and the gas equilibrium pressure inside the sample compartment were recorded. From a thermodynamic point of view, the infrared cell, used as described above, operates as a closed system; in contrast to calorimetric or volumetric adsorption measurements, which are usually performed in open systems [38]. In order to check reproducibility, and to improve accuracy, the cell was then outgassed and dosed again with CO, and a new series of variable temperature IR spectra was recorded. The same procedure was followed using dinitrogen as probe molecule in the range of 113-184 K. Transmission FTIR spectra were collected, at 3 cm^{-1} resolution, on a Bruker Vertex 80v spectrometer equipped with an MCT cryodetector; 64 scans were accumulated for each spectrum.

From the integrated absorbance of the characteristic IR absorption band, of either the adsorbed probe molecule or the adsorption complex, in a series of spectra taken over a temperature range, the standard adsorption enthalpy, ΔH^0, involved in the adsorption process can be determined following the variable-temperature IR (VTIR) method described in detail elsewhere [32,33,39]. In essence, at any given temperature, T, the integrated intensity, A, of the characteristic IR absorption band being considered should be proportional to the surface coverage, θ, thus giving information on the activity (in the thermodynamic sense) of both the adsorbed species and the empty adsorption sites, $1-\theta$. Simultaneously, the equilibrium pressure, p, provides information on the activity of the gas phase. Hence, the corresponding adsorption equilibrium constant, K, at that temperature, can be determined, and the variation of K with temperature yields the corresponding value of adsorption enthalpy. Assuming Langmuir-type adsorption, we have:

$$\theta = A/A_M = K(T)\, p \,/\, [1 + K(T)\, p] \qquad (1)$$

where A_M is the integrated intensity corresponding to full coverage ($\theta = 1$). Combination of Equation (1) with the well-known Van't Hoff Equation (2) leads to Equation (3) below:

$$K(T) = \exp(-\Delta H^0/RT)\exp(\Delta S^0/R) \quad (2)$$

$$\ln[A/(A_M-A)p] = (-\Delta H^0/RT)+(\Delta S^0/R), \quad (3)$$

from which ΔH^0 value can be obtained. The ΔS^0 value can be also determined, which depends on pressure through the gas phase entropy: the reference state for the gas is usually taken as 1 mbar, representative of the pressure at which measurements are performed [38].

3. Results

3.1. Structural and morphological characterization

Figs. 1 and 2 show the X-ray diffraction patterns of the synthesized Na-[Ga]-ZSM-5 and Na-[Al]-ZSM-5 samples, respectively. In all cases, the powder X-ray diffractograms were found to be in agreement with the powder diffraction pattern corresponding to the MFI structural type [40] and showed no presence of any other crystalline products able to be detected. This, however, does not exclude the possible presence of a small proportion of an amorphous phase which would escape detection by X-ray diffraction. The narrow diffraction peaks and their relatively high intensity reflect good crystallinity, which was not affected either by the ionic exchange or by the subsequent calcination.

As can be observed in Fig. 1c, the X-ray diffraction pattern of the Na-[Ga]-ZSM-5(75) zeolite, unlike those of the rest of the samples, shows a peak doublet for 2θ values of 24.4 and 29.9° probably consequence of a change in the symmetry of the zeolite from orthorombic to monoclinic already observed in other highly siliceous end-members of ZSM-5 zeolites [41,42]. Also the relative intensity of the (101) and (200) peaks (2θ values at 8 and 8.9°) of the X-ray diffraction patterns of [Ga]-ZSM-5 zeolites varies depending on the gallium content which, in this case, is probably due to a preferred orientation of the particles or to a different Si,Ga ordering in the framework as suggested by Liu and Klinowski [43].

To prove incorporation of gallium into the gallosilicate framework, *d* spacings of a few selected diffraction lines were measured and plotted against the corresponding Si/Ga ratio (Fig. 3). In all cases a linear variation was obtained, where *d* spacings increase when decreasing the Si/Ga ratio, which indicates an expansion of the lattice as gallium content increases. This is a direct consequence of the larger size of the Ga^{3+} ion (as compared to Si^{4+}), demonstrating the incorporation of gallium into the zeolite framework [44].

Fig. 4 shows representative scanning electron micrographs of the as synthesized materials. [Al]-ZSM-5 (Fig. 4a) zeolites show crystals having a hexagonal prism shape with an average size of about 6x6 μm, while in the case of [Ga]-ZSM-5 zeolites (Fig. 4b), the solid consists of spheroidal aggregates (ca. 15 μm) of laminar particles. Similar morphologies have been reported by other authors [9,14].

Incorporation of the gallium and aluminium in the zeolite framework, was also checked by ^{71}Ga NMR and ^{27}Al NMR spectroscopy. ^{71}Ga NMR spectra (Fig. 5) show, in all cases, a single peak (with an intensity increasing with the gallium content) at around 160 ppm which is assigned to tetrahedrally coordinated gallium species [45–48]. This fact, taken together with the absence of signals at 0 or 50 ppm, which would correspond to gallium oxide or gallium oxide-hydroxide extra-framework species, gives further prove that the gallium was incorporated (replacing silicon) in the structural skeleton of the gallosilicates. However, due to the background noise of the signal, the presence of weaker NMR signals that could be due to non-equivalent tetrahedral environments or octahedral coordinated gallium species cannot be definitely excluded. Analogous results were obtained in the case of [Al]-ZSM-5 zeolites. ^{27}Al NMR spectra show a single signal at 56 ppm corresponding to Al in a tetrahedral coordination (Fig. 6). In the case of the zeolite [Al]-ZSM-5(50), this peak shows a fine structure arising from at least two components, which has been also observed by other authors [41,49] and assigned to the presence of crystallographically non-equivalent sites for tetrahedral aluminium.

3.2. Brønsted acidity measurement by variable-temperature IR spectroscopy

Representative variable temperature IR spectra of carbon monoxide adsorbed on H-[Ga]-ZSM-5(25) in the O–H stretching region are depicted in Fig. 7a. The zeolite blank spectrum (Fig. 7a inset) shows a sharp band at 3619 cm^{-1}, which corresponds to bridging

Si(OH)Ga hydroxyl groups that constitute the Brønsted acid sites of the zeolite. This band is superimposed to a very broad and complex IR absorption feature covering the 3700-3000 cm^{-1} range, which shows a maximum at about 3500-3300 cm^{-1}. A similar band, whose intensity and shape greatly vary from one preparation to another suggesting a defective origin, has been reported by other authors [50–53]. A broad absorption in this region has also been found in defective silicalite, i.e. a silicalite sample containing a great concentration of hydroxyl nests. As a consequence, we assign the broad IR band in the 3700-3000 cm^{-1} range to the stretching vibration of hydrogen-bonded silanols in similar nests, probably formed during some of the thermal treatments which the samples are subjected to. The spectra also show weak bands in the 3750-3700 cm^{-1} region which are assigned to free (or weakly perturbed) silanols.

Interaction of the zeolite with adsorbed CO (main body of Fig. 7a) resulted in an intensity decrease of the IR absorption band at 3619 cm^{-1}, to an extent which (for a fixed CO dose) is a function of the temperature, and simultaneously a new broad band centred at 3338 cm^{-1} builds up. Clearly, this new band comes from the hydrogen bonded adsorption complex formed by the carbon monoxide and the zeolite Brønsted acid sites [**¡Error! Marcador no definido.**–53]. From the whole series of variable temperature IR spectra recorded, the Van't Hoff plot depicted in Fig. 8a was obtained, applying Eq. 3. From this linear plot, the corresponding value of the standard adsorption enthalpy involved in the formation of the OH···CO adsorption complexes resulted to be ΔH^0= -23.6 kJ mol^{-1}. The estimated error limit is of about ±2 kJ mol^{-1}.

Formation of the OH···CO hydrogen-bonded complex also resulted in the appearance in the C–O stretching region of the corresponding main IR absorption band, at 2171 cm^{-1}, as shown in Fig. 7b. After determination of the integrated IR absorbance of the band at 2171 cm^{-1} for the whole set of IR spectra recorded, the Van't Hoff plot shown in Fig. 8b was obtained. This linear plot gave the value of ΔH^0= -23.1 kJ mol^{-1}. As expected, this value is practically identical, within the experimental error, to that obtained from the Van't Hoff plot corresponding to the IR absorption band at 3619 cm^{-1}.

Spectra corresponding to the adsorption of CO on H-[Ga]-ZSM-5(50) and H-[Ga]-ZSM-5(75) in the O–H and the C–O stretching region (Figs. S1 and S3) were very similar to those of carbon monoxide adsorbed on H-[Ga]-ZSM-5(25). The only difference was the intensity of the band corresponding to the Si(OH)Ga bridged Brønsted groups which decreases with increasing Si/Ga ratio. As in the case of the H-[Ga]-ZSM-5(25) sample, after integration of the intensity of the IR absorption bands corresponding to the bridging

Si(OH)Ga hydroxyl groups and to the CO adsorbed on these groups for the whole set of IR spectra recorded, the corresponding Van't Hoff plots were obtained (Figs. S2 and S4). From these linear plots, corresponding ΔH^0 values were determined. They are summarized in Table 1.

For the sake of comparison, Brønsted acidity of two H-[Al]-ZSM-5 zeolites having different Si/Al ratio was also determined by means of variable temperature IR spectroscopy. Fig. 9 shows the O–H and C–O stretching region of carbon monoxide adsorbed on H-[Al]-ZSM-5(25). The blank spectrum of the zeolite (inset of Fig. 9a) shows a main IR absorption band at 3614 cm^{-1} corresponding to the bridging Si(OH)Al hydroxyl groups and, as in the case of H-[Ga]-ZSM-5, a less intense band (formed by more than one component) covering the 3750-3700 cm^{-1} range, which is due to silanol groups which frequently present a certain degree of heterogeneity [54]. Fig. 9a shows the expected decreased intensity of the band at 3614 cm^{-1} after the interaction with carbon monoxide, and the progressive development of the band centred at 3310 cm^{-1} coming from the hydrogen-bonded adducts which also resulted in the appearance of the corresponding IR absorption band at 2173 cm^{-1} (Fig. 9b) [54]. After determination of the integrated IR absorbance of the bands at 3614 and 2173 cm^{-1} for the whole set of IR spectra recorded, the Van't Hoff plots shown in Figs. 10a and 10b were obtained, which rendered the ΔH^0 values summarized in Table 2. As expected, ΔH^0 values derived from the O–H stretching mode and from the C–O stretching mode are coincident within experimental error. For comparison, some related data previously reported in the literature [55–57] are also shown in Table 2.

VTIR spectra obtained for CO adsorbed on H-[Al]-ZSM-5(50) were very similar to those obtained for H-[Al]-ZSM-5(25). These spectra and the derived Van't Hoff plots can be found in the supplementary information (Figs. S5 and S6). The corresponding set of obtained results are summarized in Table 2.

For completion, relative Brønsted acidity of the gallosilicate and aluminosilicate samples discussed above, was also determined by using dinitrogen as the IR probe molecule. Corresponding VTIR spectra and Van't Hoff plots for the H-[Ga]-ZSM-5(25) and H-[Al]-ZSM-5(25) samples are shown in Figs. from 11 to 14. Numerical values are summarized in Tables 1 and 2.

As in the case of CO, upon interaction of the H-[Ga]-ZSM-5(25) with adsorbed dinitrogen, the Brønsted acid Si(OH)Ga band at 3619 cm^{-1} is increasingly eroded when

the temperature is decreased (Fig. 11a). Simultaneously, a new IR absorption band appears at 3517 cm^{-1} due to the formation of the corresponding dinitrogen adsorption complexes. The corresponding N–N stretching vibrational mode (rendered IR active by the perturbation caused by adsorption) appears at 2331 cm^{-1} (Fig. 11b) [58]. The Van't Hoff plot obtained using the integrated intensity of the Si(OH)Ga band at 3619 cm^{-1} gave a straight line which rendered a ΔH^0 value of -15.8 kJ mol^{-1} (Fig. 12a), which is the same, within the experimental error, as that given by the Van't Hoff plot obtained using the IR absorption band at 2331 cm^{-1} which was of -15.4 kJ mol^{-1} (Fig. 12b).

Fig. 13a shows that, also in the case of adsorption of dinitrogen on the H-[Al]-ZSM-5(25) sample, the decrease in temperature results in the progressive erosion of the band at 3614 cm^{-1} and the parallel growth of a new band with a maximum at 3500 cm^{-1} due to the formation of hydrogen bonded OH···N_2 adducts [58]. The characteristic IR absorption band of the IR activated N–N stretching mode appeared at 2332 cm^{-1} (Fig. 13b). From Van't Hoff plots (Fig. 14), ΔH^0 of H-bond formation between dinitrogen and the Brønsted acid sites of the zeolite were determined, obtaining the following values: ΔH^0= -19.7 kJ mol^{-1} in the case of using the integrated intensity of the Si(OH)Al band at 3614 cm^{-1}, and ΔH^0= -19.5 kJ mol^{-1} when using the band at 2332 cm^{-1}, which are practically the same taking into account experimental error.

The standard enthalpy and entropy change involved in the interaction of dinitrogen and Brønsted acid sites of the other H-[Ga]-ZSM-5 and H-[Al]-ZSM-5 samples were determined following the same procedure described above (Figs. S7-S12) and the results are summarized in Tables 1 and 2.

4. Discussion

Regarding aluminosilicates, both, the red shift of the O-H stretching wavenumber ($\Delta\bar{\upsilon}_{OH}$) after the adsorption of carbon monoxide and dinitrogen on the bridging hydroxyl groups, and the standard enthalpy change involved in hydrogen bonding of Brønsted-acid hydroxyl groups with adsorbed CO and N_2, correspond very well to the values already published for zeolites belonging to the same structural type [39,55–57] as shown in Table 2. Otero Areán et al. [55] studied the adsorption of carbon monoxide and dinitrogen on a H-[Al]-ZSM-5 zeolite with a Si/Al ratio of 30 by VTIR spectroscopy. The standard enthalpy was found to be −29.4 and −19.7 kJ mol^{-1} for the adsorption of CO and N_2, respectively; values that are (within experimental error) practically the same as those

obtained in the present work. Very similar too are the values reported by Savitz et al. [56] who, by using calorimetric techniques, obtained standard enthalpy values of −27 and −16 kJ mol^{-1} for the adsorption of CO and N_2, respectively, on a H-[Al]-ZSM-5 zeolite with a Si/Al ratio of 27. Recently, it has been reported that the heat of adsorption of molecules, like CO, N_2, CO_2 or CH_4, on the Brønsted acid sites of zeolites is influenced by the local environment of the site and by the measurement temperature [59−62], finding differences of more than 15 kJ mol^{-1} depending on the molecule adsorbed, the heterogeneity of the sites present in the material or the temperature range studied. It should be kept in mind that the temperature range over which measurements are run in our case is much narrower in comparison to that studied in the previous reports so that standard entropy and enthalpy changes may be considered as being practically constant. However, in light of the previously reported results, the standard adsorption enthalpy values here reported probably represent average ΔH^0 values for the formation of CO and N_2 adsorption complexes on the different acid sites and over the temperature range spanned.

In the case of gallosilicates, as far as we know, the standard adsorption enthalpies of carbon monoxide or dinitrogen in this type of materials have never been reported before. However, the acidity of [Ga]-ZSM-5 zeolites has been studied by IR spectroscopy of CO and N_2 adsorbed at 77 K [50] using the red shift of the O-H stretching frequency in the hydrogen-bonded OH· · ·CO or OH· · ·N_2 complexes formed after CO and N_2 adsorption as a measurement of the relative acidity strength. Table 1 summarizes the most relevant data corresponding to the spectroscopic and thermodynamic study carried out in the present work for the CO/[Ga]-ZSM-5 and N_2/[Ga]-ZSM-5 systems with different Si/Ga ratios (25, 50, and 75), as well as the previously published values of the bathochromic shift of the O−H stretching wavenumber after the adsorption of CO and N_2 on Brønsted acid sites of a H-[Ga]-ZSM-5.

On account of simplicity, the magnitude of the red shift of the O–H stretching frequency ($\Delta\upsilon_{(OH)}$) when the Brønsted-acid hydroxyl group of protonic zeolites interacts with an adsorbed weak base (such as carbon monoxide or dinitrogen) is frequently used for ranking zeolite acid strength [63−65]; the stronger the Brønsted acid site, the larger the value of $\Delta\upsilon_{(OH)}$ (for any given weak base). However, it has recently been shown that the value of ΔH^0 is a more reliable indicator of the Brønsted acid strength of proton zeolites [30−32].

In both cases, aluminosilicates and gallosilicates belonging to the MFI structural type, previous reports [53,56,65,66] showed that the bathochromic shift of the O–H

stretching mode, $\Delta\upsilon_{(OH)}$, determined using CO or N_2 as the probe molecule is smaller for gallosilicates than for aluminosilicates. And that is also the case for the adsorption enthalpy values reported herein (Tables 1 and 2), which are distinctively lower in the case of the gallosilicates. Thus, for CO adsorption, the average ΔH^o value of ≈−29 kJ mol^{-1} was obtained in the case of H-[Al]-ZSM-5 zeolites, to be compared with that of ≈−23.5 kJ mol^{-1} for the gallosilicates. And the same trend was observed for the dinitrogen: ΔH^o ≈−20 kJ mol^{-1} in the case of aluminosilicates, and ΔH^o≈−15 kJ mol^{-1} for the gallosilicates, proving the lower Brønsted acid strength of the bridging hydroxyl groups of the H-[Ga]-ZSM-5 gallosilicates compared to that of the Brønsted acid sites of H-[Al]-ZSM-5 aluminosilicates.

Finally, it is noteworthy that within the composition range investigated (Si/Al or Si/Ga ratio between 25 and 75) the Brønsted acid strength of both, aluminosilicates and gallosilicates, is independent of the Si/T ratio (T= Al, Ga) regardless of which indicator is used to measure acidity, the red shift of the O–H stretching frequency, $\Delta\upsilon_{(OH)}$, or the standard adsorption enthalpy, ΔH^o. In the case of the zeolites, which have been studied in a greater extent than gallosilicates, it is known that the Brønsted acid strength increases when the aluminium content decreases; however, there is a limit above which the acid strength remains constant even if the Si/Al ratio continues to be increased [67]. This experimental fact, corroborated herein, shows that a determining factor of acid strength is the local environment of the Si(OH)T Brønsted acid group, and more specifically the number of TO_4 tetrahedra present in its second coordination sphere of the T atom [68,69]. The high Si/Ga ratio of the gallosilicates studied herein explains the constant value of their Brønsted acid strength, since the Si(OH)Ga units are highly unlikely to be in close contact to one another.

5. Conclusions

The Brønsted acid strength of H-[Ga]-ZSM-5 gallosilicates having Si/Ga ratio of 25, 50 and 75 was determined by variable-temperature IR (VTIR) spectroscopy using carbon monoxide and dinitrogen as probe molecules. This allowed us to obtain simultaneously the bathochromic shift, $\Delta\upsilon_{(OH)}$, of the hydrogen-bonded O–H···CO (O–H···N_2) adsorption complex with the Brønsted acid site and the corresponding standard adsorption enthalpy change, ΔH^o, involved in the gas adsorption process. Independently of their Si/Ga ratio, the protonic gallosilicates showed the value of $\Delta\upsilon_{(OH)}$ =−280 (±1) cm^{-1} and ΔH^o=−23 (±2) kJ mol^{-1} for CO, and $\Delta\upsilon_{(OH)}$ =−102 (±2) cm^{-1} and ΔH^o=−15 (±2) kJ mol^{-1} for N_2.

For comparative purposes, the Brønsted acidity of H-[Al]-ZSM-5 protonic aluminosilicates having Si/Al ratios of 25 and 50 was also determined. The results obtained were $\Delta\upsilon_{(OH)}$ =−305 cm^{-1} and ΔH^{o}=−29.3 (±2) kJ mol^{-1} using CO as the probe molecule; and $\Delta\upsilon_{(OH)}$=−115 cm^{-1} and ΔH^{o}=−19.7 (±2) kJ mol^{-1} using N_2, in both cases independently of the Si/Al ratio of the aluminosilicates. Comparison between the corresponding values shown by the gallosilicates and by the aluminosilicates proves the lower acid strength of the former, independently of the acidity indicator used: $\Delta\upsilon_{(OH)}$ or ΔH^{o}. This is a relevant finding because, as recently reported [30,31], $\Delta\upsilon_{(OH)}$ and ΔH^{o} not always correlate among themselves when used as indicators to rank Brønsted acid strength of zeolites.

References

[1] C.T.-W. Chu, C.D. Chang, J. Phys. Chem. 89 (1985) 1569.
[2] J. Čejka, A. Vondrová, B. Wichterlová, G. Vorbeck, R. Fricke, Zeolites 14 (1994) 147.
[3] S.P. Yuan, J.G. Wang, Y.W. Li, H. Jiao, J.Phys. Chem. A 106 (2002) 8167.
[4] M.V. Shamzhy, O.V. Shvets, M.V. Opanasenko, P.S. Yaremov, L.G. Sarkisyan, P. Chlubná, A. Zukal, R. Marthala, M. Hartmann, J. Čejka, J. Mater. Chem. 22 (2012) 15793.
[5] J.R. Mowry, R.F. Anderson, J.A. Johnson, Oil Gas J. 83 (1985) 128.
[6] R. Fricke, H. Kosslick, G. Lischke, M. Richter, Chem. Rev. 100 (2000) 2303.
[7] K.E. Ogunronbi, N. Al-Yassir, S. Al-Khattaf. J. Mol. Catal. A Chem. 406 (2015) 1.
[8] I. Nakamura, K. Fujimoto, Catal. Today 31 (1996) 335.
[9] X. Su, G. Wang, X. Bai, W. Wu, L. Xiao, Y. Fang, J. Zhang, Chem. Eng. J. 293 (2016) 365.
[10] Y. Fang, X. Su, X. Bai, W. Wu, G. Wang, L. Xiao, A. Yu, J. Ener. Chem. 26 (2017) 768.
[11] A. Samanta, X. Bai, B. Robinson, H. Chen, J. Hu, Ind. Eng. Chem. Res. 56 (2017) 11006.
[12] J. Li, Y. Yu, X. Li, W. Wang, G. Yu, S. Deng, J. Huang, B. Wang, Y. Wang, Appl. Catal. B: Environ. 172–173 (2015) 154.
[13] V.B. Kumar, I.N. Pulidindi, R.K. Mishra, A. Gedanken, ChemistrySelect 1 (2016) 5952.
[14] L.H. Vieira, K.T.G. Carvalho, E.A. Urquieta-González, S.H. Pulcinelli, C. V. Santilli, L. Martins, J. Mol. Catal. A: Chem. 422 (2016) 148.
[15] W. Zhou, M. Liu, Q. Zhang, Q. Wei, S. Ding, Y. Zhou, ACS Catal. 7 (2017) 7665.
[16] M. Guisnet, N.S. Gnep, Catal. Today 31 (1996) 275.
[17] V.R. Choudhary, K. Mantri, C. Sivadinarayana, Microporous Mesoporous Mater. 37 (2000) 1.
[18] H. Xiao, J. Zhang, P. Wang, Z. Zhang, Q. Zhang, H. Xie, G. Yang, Y. Han, Y. Tan, RSC Adv. 5 (2015) 92222.
[19] V.R. Choudhary, A.K. Kinage, C. Sivadinarayana, P. Devadas, S.D. Sansare, M. Guisnet, J.Catal. 158 (1996) 34.

[20] A. Aloise, E. Catizzone, M. Migliori, J.B. Nagy, G. Giordano, Chin. J. Chem. Eng. 25 (2017) 1863.
[21] S.-W. Choi, W.-G. Kim, J.-S. So, J.S. Moore, y. Liu, R.S. Dixit, J.G. Pendergast, C. Sievers, D.S. Sholl, S. Nair, C.W. Jones, J. Catal. 345 (2017) 113.
[22] M. Xin, E. Xing, X. Gao, Y. Wang, Y. Ouyang, G. Xu, Y. Luo, X. Shu, Ind. Eng. Chem. Res. 58 (2019) 6970.
[23] E.G. Derouane, J.C. Védrine, R. Ramos Pinto, P.M. Borges, L. Costa, M.A.N.D.A. Lemos, F. Lemos, F. Ramôa Ribeiro, Catal. Rev. Sci. Eng. 55 (2013) 454.
[24] M. Boronat, A. Corma, Catal. Lett. 145 (2015) 162.
[25] L.E. Sandoval-Díaz, J.A. González-Amaya, C.A. Trujillo, Micropor.Mesopor. Mater. 215 (2015) 229.
[26] A. Zecchina, C. Lamberti, S. Bordiga, Catal. Today. 41 (1998) 169.
[27] A. Zecchina, G. Spoto, S. Bordiga, Phys. Chem. Chem. Phys. 7 (2005) 1627.
[28] K. Chakarova, K. Hadjiivanov, Chem. Commun. 47 (2011) 1878.
[29] K. Chakarova, K. Hadjiivanov. J. Phys. Chem. C 115 (2011) 4806.
[30] Montserrat R. Delgado, Roman Bulánek, Pavla Chlubná, Carlos O. Arean, Catal. Today 227 (2014) 45.
[31] C.O. Arean, M.R. Delgado, P. Nachtigall, H. Viet Thang, M. Rubeš, R. Bulánek, P. Chlubná-Eliášová, Phys. Chem. Chem. Phys. 16 (2014) 10129.
[32] C.O. Arean, Ukr. J. Phys. 63 (2018) 538.
[33] E. Garrone, C.O Arean, Chem. Soc. Rev. 34 (2005) 846.
[34] C.O Arean, D. Nachtigallová, P. Nachtigall, E. Garrone, M.R. Delgado, Phys. Chem. Chem. Phys. 9 (2007) 1421
[35] D.K. Simmons, R. Szostak, P.K. Agrawal, J. Catal. 106 (1987) 287.
[36] L.D. Rollman, E.W. Valyocsik, Inorganic Synthesis 22 (1983) 61.
[37] A.A. Tsyganenko, P.Y. Storozhev, C.O. Arean, Kinet. Catal. 45 (2004) 530.
[38] E. Garrone, M.R. Delgado, B. Bonelli, C.O. Arean, Molecules 22 (2017) 1557.
[39] C.O. Arean, O. V. Manoilova, G.T. Palomino, M.R. Delgado, A.A. Tsyganenko, B. Bonelli, E. Garrone, Phys. Chem. Chem. Phys. 4 (2002) 5713.
[40] D.H. Baerlocher, C. McCusker, L.B. Olson, Atlas of Zeolite Framework Type, Elsevier, Amsterdam (2007).
[41] C.A. Fyfe, G.C. Gobbi, J. Klinowski, J.M. Thomas, S. Ramdas, Nature 296 (1982) 530.
[42] D.G. Hay, H. Jaeger, J. Chem. Soc., Chem. Commun. (1984) 1433.
[43] X. Liu, J. Klinowski, J. Phys. Chem. 96 (1992) 3403.
[44] D.M. Bibby, L.P. Aldridge, N.B. Milestone, J. Catal.72 (1981) 373.
[45] H.K.C. Timken, E. Oldfield, J. Am. Chem. Soc. 109 (1987) 7669.
[46] C.R. Bayense, A.P.M. Kentgens, J.W. De Haan, L.J.M. Van de Ven, J.H.C. VanHooff, J. Phys. Chem. 96 (1992) 775.
[47] C. Bigey, B.L. Su, J. Mol. Catal. A: Chem. 209 (2004) 179.
[48] M. Hunger, E. Brunner, NMR Spectroscopy. In: H.G.Karge, J. Weitkamp (eds) Characterization of Molecular Sieves. vol.4 p.201.Springer, Berlin (2004).
[49] C.A. Fyfe, J.M. Thomas, J. Klinowski, G.C. Gobbi, Angew. Chem. Int. Ed. 22 (1983) 259.
[50] C.O. Arean, G.T. Palomino, F. Geobaldo, A. Zecchina, J. Phys. Chem. 100 (1996) 6678.
[51] G.E. Ewing, G.C. Pimentel, J. Chem. Phys. 35 (1961) 925.
[52] A.Y. Khodakov, L.M. Kustov, T.N. Bondarenko, A.A. Dergachev, V.B. Kazansky, K.M. Minachev, H.K. Beyer, Zeolites 10 (1990) 603.

[53] A. Zecchina, S. Bordiga, G. Spoto, D. Scarano, G. Petrini, G. Leofanti, M. Padovan, C.O. Arean, J. Chem. Soc. Faraday Trans. 88 (1992) 2959.
[54] A. Zecchina, C.O. Arean, Chem. Soc. Rev. 25 (1996) 187.
[55] C.O. Arean, J. Mol. Struct. 880 (2008) 31.
[56] S. Savitz, A.L. Myers, R.J. Gorte, Microporous Mesoporous Mater. 37 (2000) 33.
[57] F. Wakabayashi, J.N. Kondo, K. Domen, C. Hirose, J. Phys. Chem. 99 (1995) 10573.
[58] L. Koubi, M. Blain, E.C. de Lara, J.M. Leclerq, Chem. Phys. Lett. 217 (1994) 544.
[59] M. Boronat, A. Corma, ACS Catalysis 9 (2019) 1539.
[60] H.V. Thang, J. Vaculin, J. Prech, M. Kubu, J. Čejka, P. Nachtigall, R. Bulanek, L. Grajciar, Microporous Mesoporous Mater. 282 (2019) 121.
[61] M. Rubes, M. Trachta, E. Kouelkova, R. Bulanek, J. Klimer, P. Nachtigall, O. Bludsky, J. Phys. Chem. C 122 (2018) 26088.
[62] A.S. Hyla, H. Fang, S.E. Boulfelfel, G. Muraro, C. Paur, K. Strohmaier, P.I. Ravikovitch, D.S. Sholl, J. Phys. Chem. C 123 (2019) 20405.
[63] K. Hadjiivanov, Adv. Catal 57 (2014) 99.
[64] M.A. Makarova, K.M. Al-Ghefaili, J. Dwyer, J. Chem. Soc. Faraday Trans. 90 (1994) 383.
[65] M.V. Frash, M.A. Makarova, A.M. Rigby, J. Phys. Chem. B 101 (1997) 2116.
[66] K.M. Neyman, P. Strodel, S.P. Ruzankin, N. Schlensog, H. Knözinger, N. Rösch, Catal. Lett. 31 (1995) 273.
[67] D. Bartomeuf, Mater. Chem. Phys. 17 (1987) 49.
[68] B. Gil, E. Broclawik, J. Datka, J. Klinowski, J. Phys. Chem. 98 (1994) 930.
[69] L. Grajciar, C.O. Arean, A. Pulido, P. Nachtigall, Phys. Chem. Chem. Phys. 12 (2010) 1497.

Figures and tables

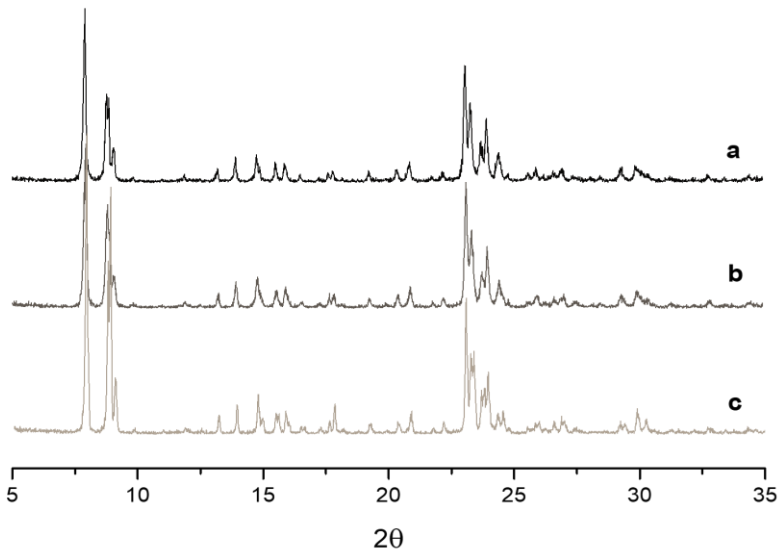

Fig.1. X-ray diffraction patterns (CuK_α radiation) of the gallosilicates (a) Na-[Ga]-ZSM-5(25), (b) Na-[Ga]-ZSM-5(50) and (c) Na-[Ga]-ZSM-5(75).

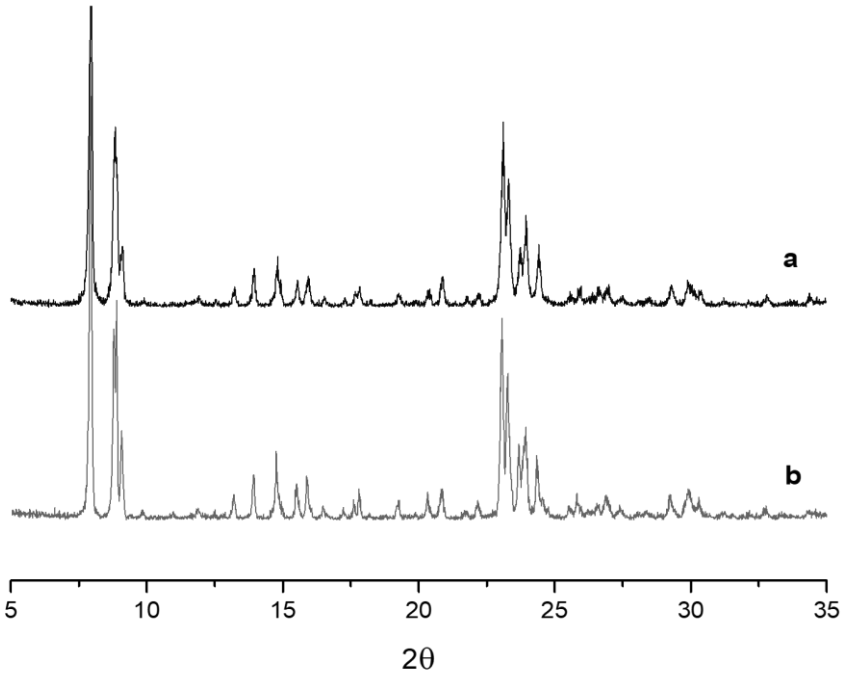

Fig.2. X-ray diffraction patterns (CuK_α radiation) of the aluminosilicates (a) Na-[Al]-ZSM-5(25) and (b) Na-[Al]-ZSM-5(50).

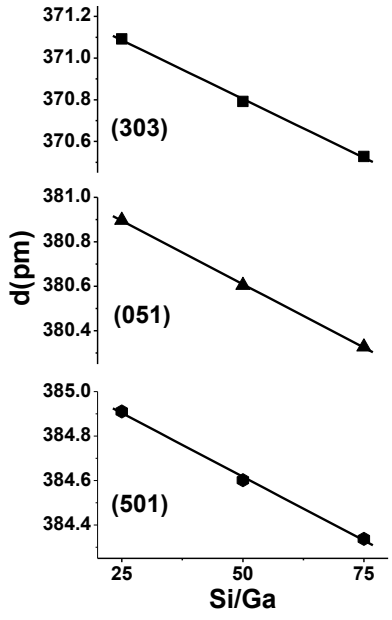

Fig.3. Variation of the interplanar spacings *d* of the diffraction lines (501), (051) and (303) with the gallium content of the samples Na-[Ga]-ZSM-5(25), Na-[Ga]-ZSM-5(50) and Na-[Ga]-ZSM-5(75).

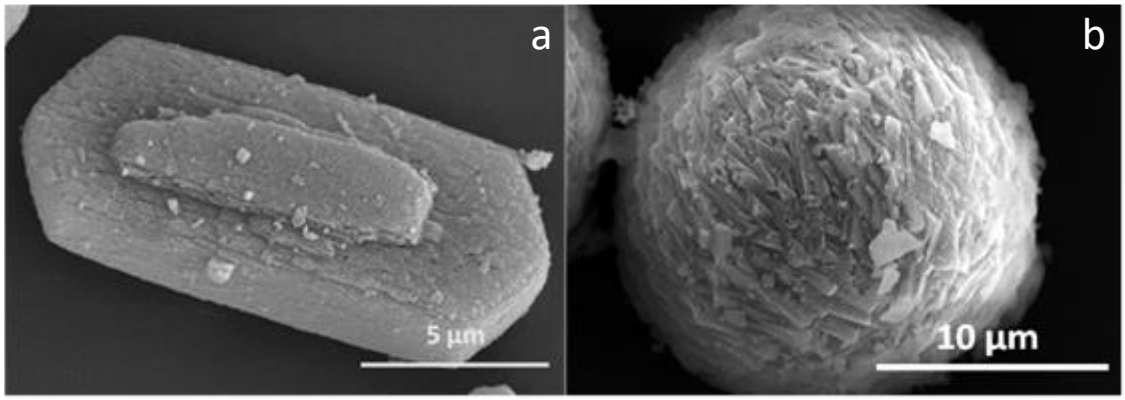

Fig.4. SEM images of the zeolites (a) Na-[Al]-ZSM-5(25) and (b) Na-[Ga]-ZSM-5(25).

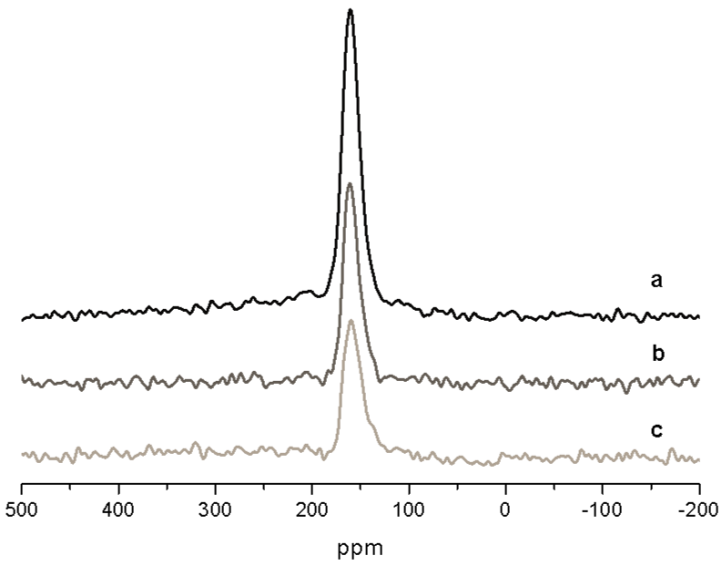

Fig.5. ^{71}Ga MAS NMR spectra of the gallosilicates (a) Na-[Ga]-ZSM-5(25), (b) Na-[Ga]-ZSM-5(50) and (c) Na-[Ga]-ZSM-5(75).

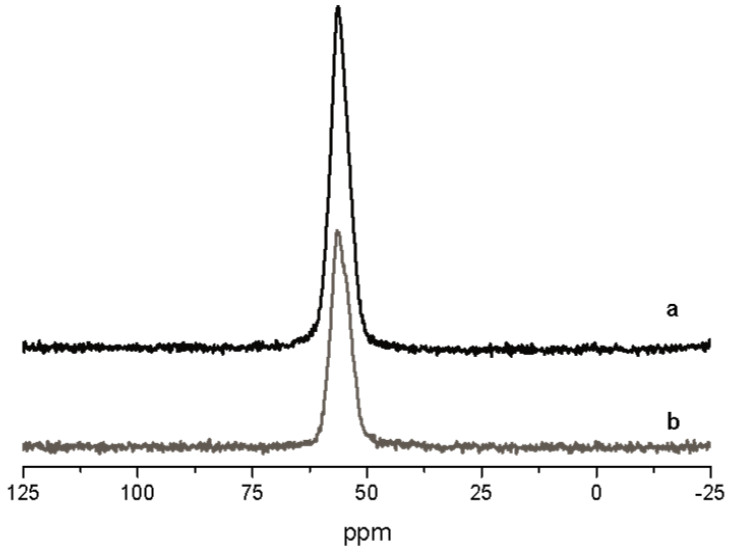

Fig.6. ^{27}Al MAS NMR spectra of the zeolites (a) Na-[Al]-ZSM-5(25) and (b) Na-[Al]-ZSM-5(50).

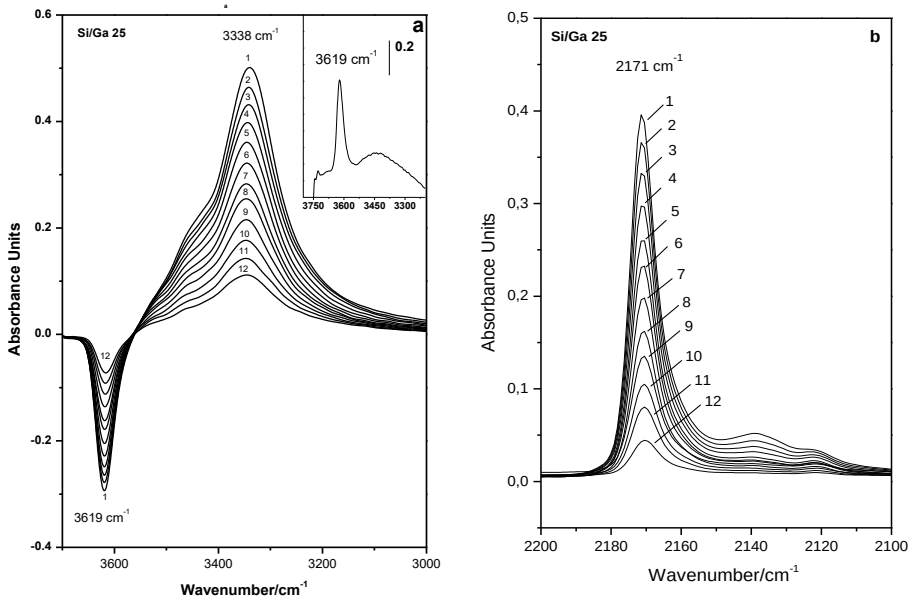

Fig.7. (a) Representative variable-temperature IR spectra (O−H stretching region) of adsorbed CO on H-[Ga]-ZSM-5(25). The spectra are shown in the difference mode (gallosilicate blank subtracted). From 1 to 12, temperature goes from 157 to 208 K and equilibrium pressure from 12.2 to 17.5 mbar. The inset shows the gallosilicate blank spectrum. (b) C−O stretching region.

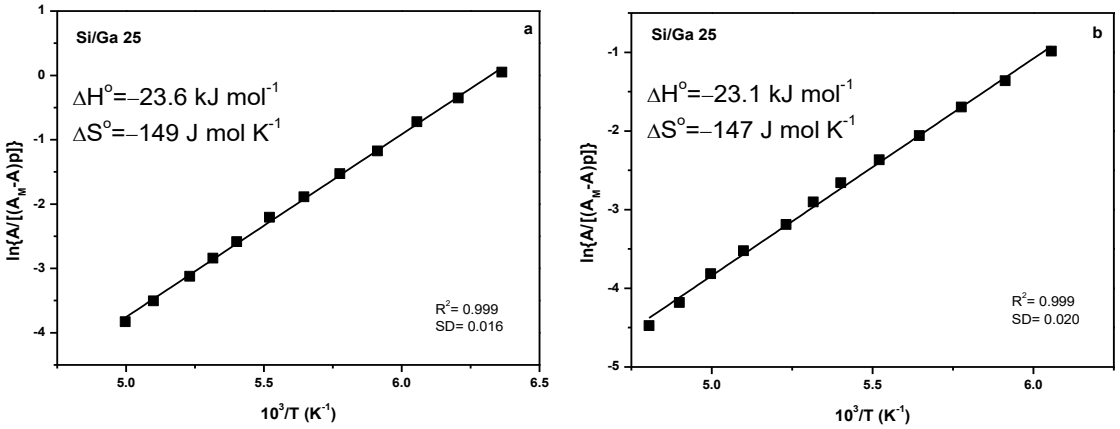

Fig.8. Plot of left-hand side of Eq. 3 against the reciprocal of the temperarure for CO adsorbed on H-[Ga]-ZSM-5(25). (a) O−H stretching region. (b) C−O stretching region. R linear regression coefficient, SD standard deviation.

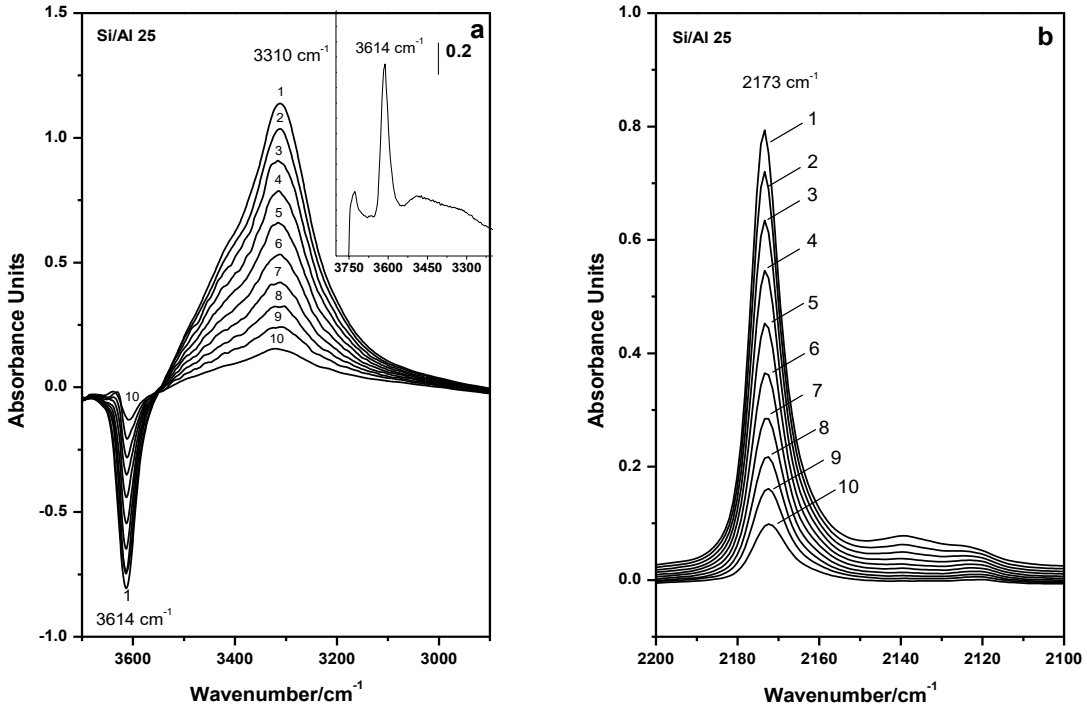

Fig.9. (a) Representative variable-temperature IR spectra (O−H stretching region) of adsorbed CO on H-[Al]-ZSM-5(25). The spectra are shown in the difference mode (aluminosilicate blank

subtracted). From 1 to 10, temperature goes from 171 to 228 K and equilibrium pressure from 11.4 to 17.6 mbar. The inset shows the aluminosilicate blank spectrum. (b) C−O stretching region.

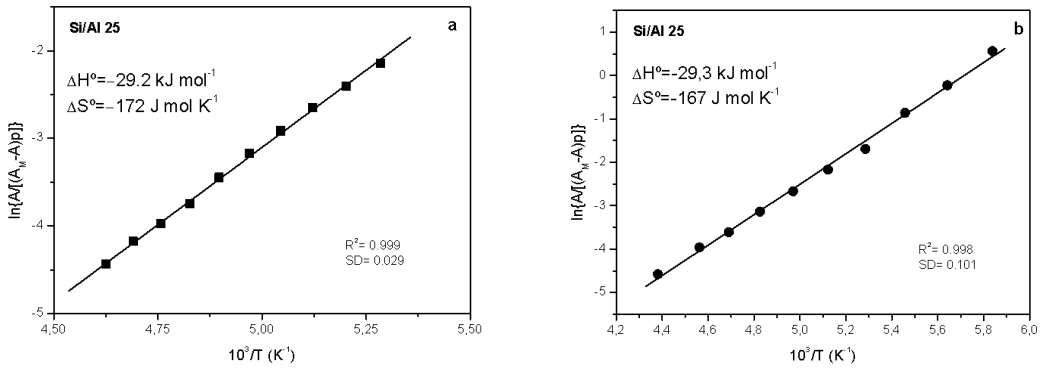

Fig.10. Plot of left-hand side of Eq. 3 against the reciprocal of the temperarure for CO adsorbed on H-[Al]-ZSM-5(25). (a) O−H stretching region. (b) C−O stretching region. R linear regression coefficient, SD standard deviation.

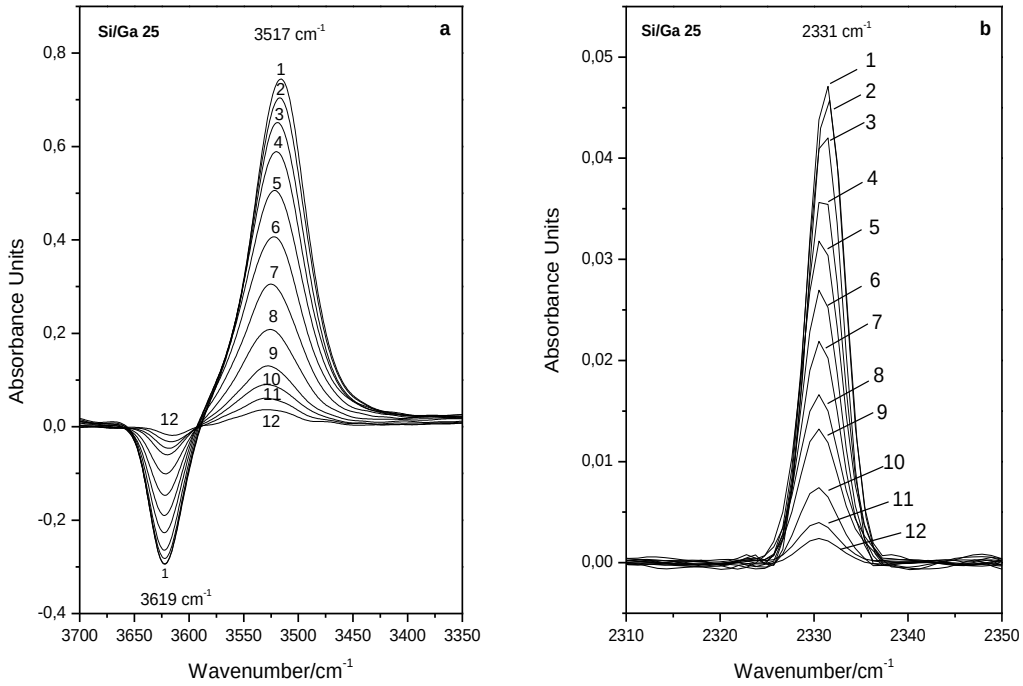

Fig.11. (a) Representative variable-temperature IR spectra (O−H stretching region) of adsorbed N_2 on H-[Ga]-ZSM-5(25). The spectra are shown in the difference mode (b) N−N stretching region. From 1 to 12, temperature goes from 118 to 165 K and equilibrium pressure from 1.2 to 9.5 mbar.

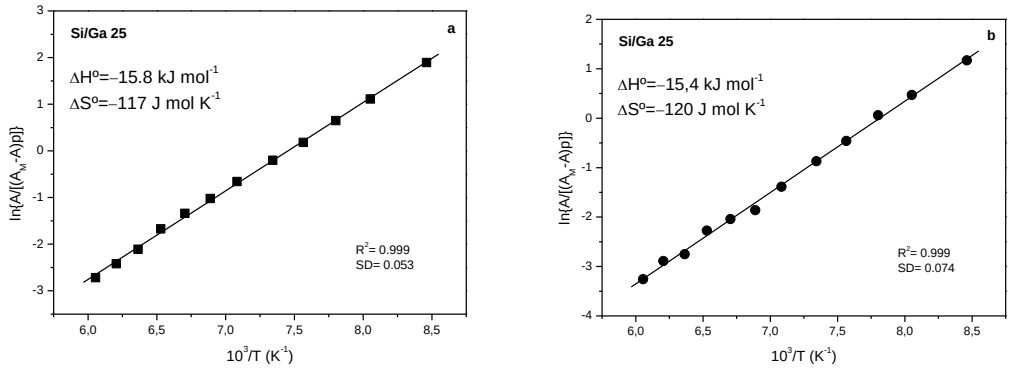

Fig.12. Plot of left-hand side of Eq. 3 against the reciprocal of the temperarure for N_2 adsorbed on H-[Ga]-ZSM-5(25). (a) O−H stretching region (b) N−N stretching region. R linear regression coefficient; SD standard deviation.

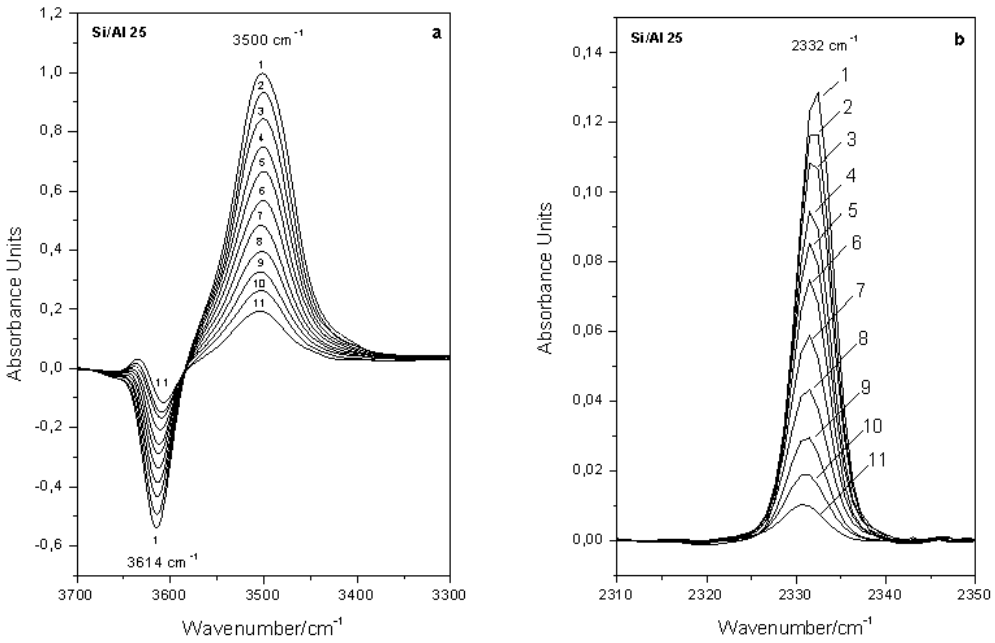

Fig.13. (a) Representative variable-temperature IR spectra (O−H stretching region) of adsorbed N_2 on H-[Al]-ZSM-5(25). The spectra are shown in the difference mode. (b) N−N stretching region. From 1 to 11, temperature goes from 123 to 184 K and equilibrium pressure from 0.29 to 4.56 mbar.

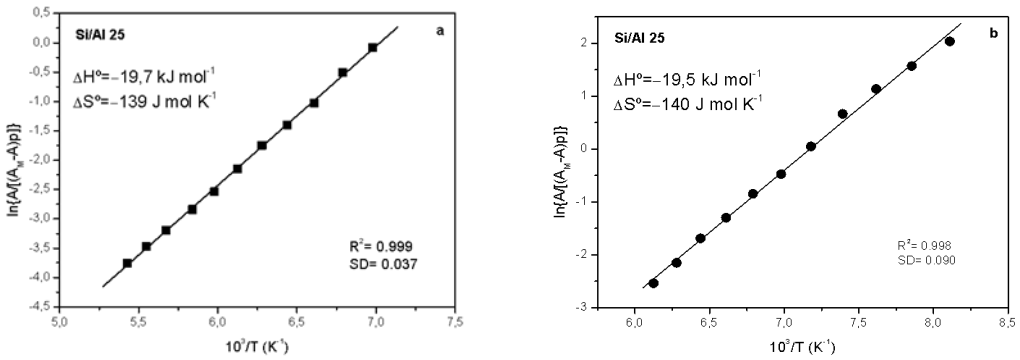

Fig.14. Plot of left-hand side of Eq. 3 against the reciprocal of the temperarure for N_2 adsorbed on H-[Al]-ZSM-5(25). (a) O−H stretching region (b) N−N stretching region. R linear regression coefficient; SD standard deviation.

Table 1. Comparison of values of ΔH^0 and $\Delta\upsilon_{OH}$ of CO and N_2 adsorbed on H-[Ga]-ZSM-5 gallosilicates (interaction of the adsorbed molecule with the Brønsted acid sites).

Sample	Si/ Ga Ratio	$\Delta\upsilon_{OH}$(CO) (cm^{-1})	$\Delta\upsilon_{OH}$(N_2) (cm^{-1})	ΔH^0(CO)* (kJ mol^{-1})	ΔH^0(N_2)* (kJ mol^{-1})	Ref.
H-[Ga]-ZSM-5(25)	25	-281	-102	-23.4	-15.6	This study[a]
H-[Ga]-ZSM-5(50)	50	-279	-104	-23.7	-15.3	This study[a]
H-[Ga]-ZSM-5(75)	75	-281	-101	-23.6	-15.4	This study[a]
H-[Ga]-ZSM-5	25	-279	-100	-	-	[50][b]

[a]VTIR; [b]FTIR.
*Enthalpy data correspond to the mean of the values obtained from variable-temperature IR spectra. Experimental error limit of values of $\perp H^0$: ±2 kJ mol^{-1}.

Table 2. Comparison of values of ΔH^0 and $\Delta\upsilon_{OH}$ of CO and N_2 adsorbed on zeolites H-[Al]-ZSM-5 (interaction of adsorbed molecule with the Brønsted acid sites).

Sample	Si/Al Ratio	$\Delta\upsilon_{OH(CO)}$ (cm^{-1})	$\Delta\upsilon_{OH(N_2)}$ (cm^{-1})	$\Delta H^0(CO)$* (kJ mol^{-1})	$\Delta H^0(N_2)$* (kJ mol^{-1})	Ref.
H-[Al]-ZSM-5(25)	25	-304	-114	-29.3	-19.6	This study[(a)]
H-[Al]-ZSM-5(50)	50	-305	-115	-29.2	-19.8	This study[(a)]
H-[Al]-ZSM-5	30	-303	-116	-29.4	-19.7	[55][a]
H-[Al]-ZSM-5	27	-	-	-27±1	-16±1	[56][b]
H-[Al]-ZSM-5	27	-307	-112	-	-	[57][c]

[a] VTIR; [b] Calorimetry ,[c] FTIR.
*Enthalpy data correspond to the mean of the values obtained from variable-temperature IR spectra. Experimental error limit of values of ΔH^0: ±2 kJ mol^{-1}.

Supplementary information

Table S1. Amounts of reagents used in the synthesis of aluminosilicates and gallosilicates samples.

Sample	Na_2SiO_3 (g)	$NaAlO_2$ (g)	$Ga(NO_3)_3$ (g)	$C_{12}H_{28}NBr$ (g)	H_2O (g)	Si/ T* gel ratio	Si/ T* ratio**
[Ga]-ZSM-5(25)	1.50	-	0.122	0.42	30	25	23
[Ga]-ZSM-5(50)	1.50	-	0.061	0.42	30	50	48
[Ga]-ZSM-5(75)	1.50	-	0.042	0.42	30	75	72
[Al]-ZSM-5(25)	4.20	0.106	-	0.88	30	25	24
[Al]-ZSM-5(50)	4.20	0.053	-	0.88	30	50	49

*T = Al or Ga.
** Determined by X-ray Fluorescence.

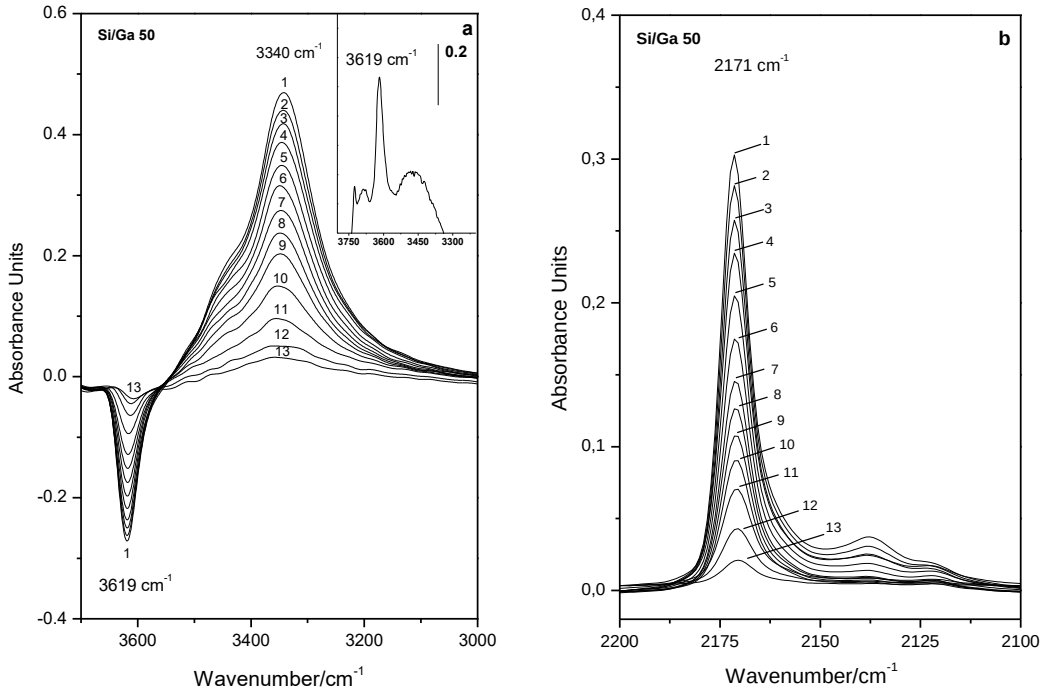

Fig.S1. (a) Representative variable-temperature IR spectra (O−H stretching region) of adsorbed CO on H-[Ga]-ZSM-5(50). The spectra are shown in the difference mode (gallosilicate blank subtracted). From 1 to 13, temperature goes from 163 to 201 K and equilibrium pressure from 5.8 to 8.1 mbar. The inset shows the gallosilicate blank spectrum. (b) C−O stretching region.

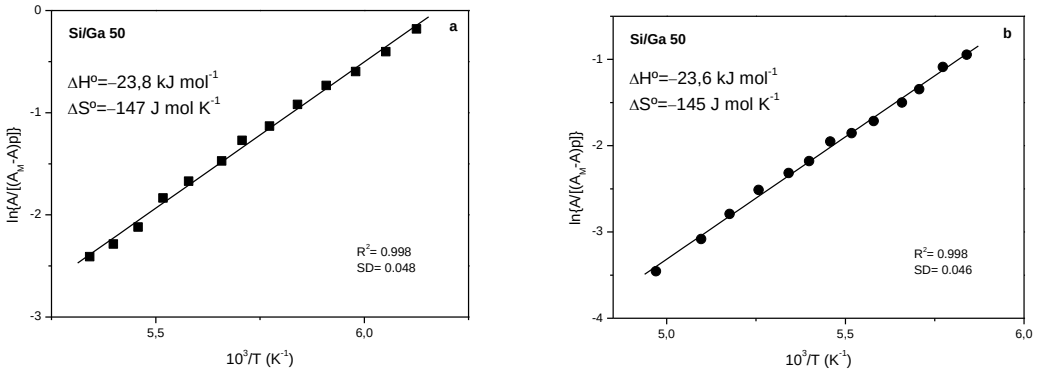

Fig.S2. Plot of left-hand side of Eq. 3 against the reciprocal of the temperarure for CO adsorbed on H-[Ga]-ZSM-5(50). (a) O−H stretching region. (b) C−O stretching region. R linear regression coefficient, SD standard deviation.

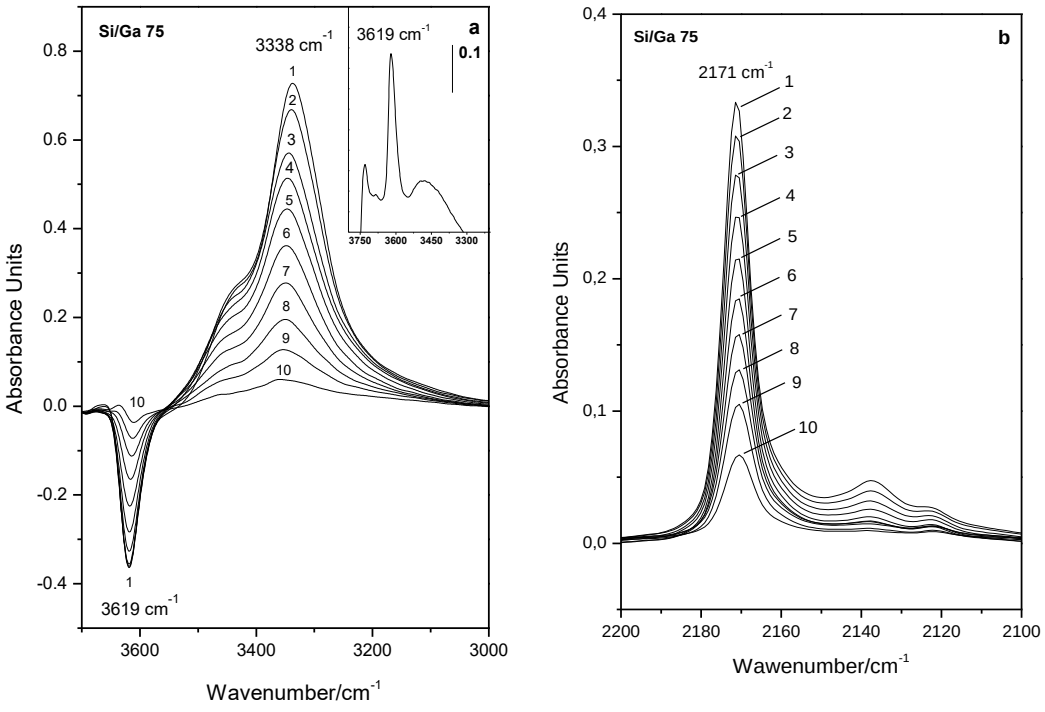

Fig.S3. (a) Representative variable-temperature IR spectra (O−H stretching region) of adsorbed CO on H-[Ga]-ZSM-5(75). The spectra are shown in the difference mode (gallosilicate blank subtracted). From 1 to 10, temperature goes from 163 to 203 K and equilibrium pressure from 5.4 to 8.1 mbar. The inset shows the gallosilicate blank spectrum. (b) C−O stretching region.

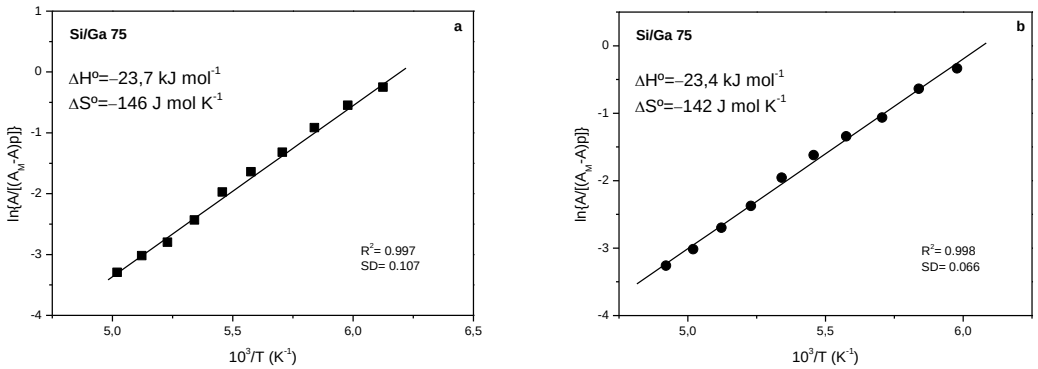

Fig.S4. Plot of left-hand side of Eq. 3 against the reciprocal of the temperarure for CO adsorbed on H-[Ga]-ZSM-5(75). (a) O−H stretching region. (b) C−O stretching region. R linear regression coefficient, SD standard deviation.

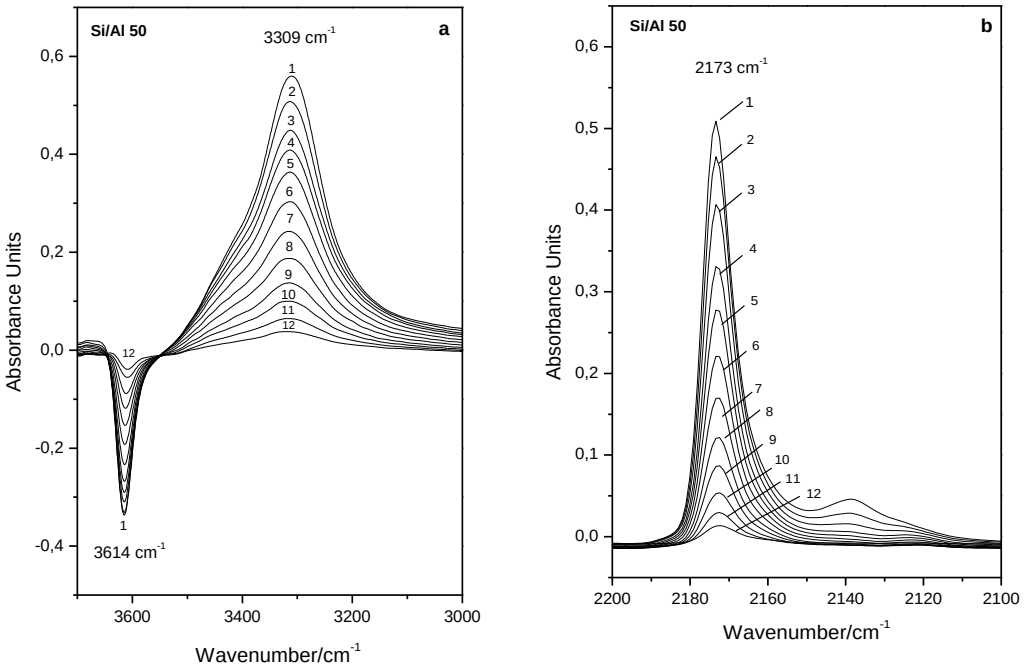

Fig.S5. (a) Representative variable-temperature IR spectra (O−H stretching region) of adsorbed CO on H-[Al]-ZSM-5(50). The spectra are shown in the difference mode. (b) C−O stretching region. From 1 to 12, temperature goes from 168 to 205 K and equilibrium pressure from 3.6 to 5.3 mbar.

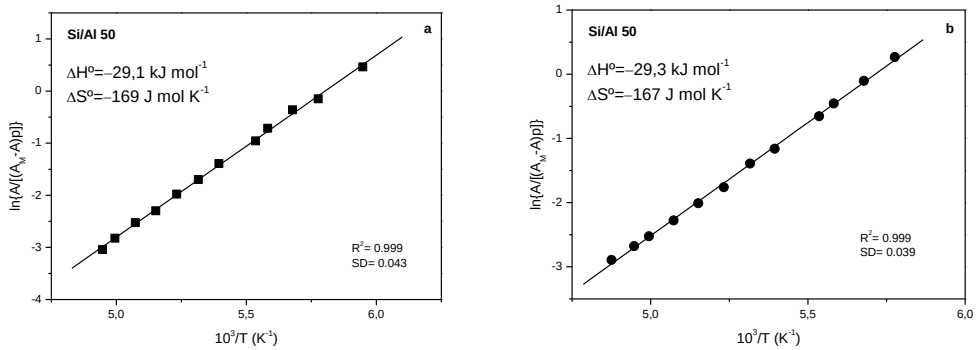

Fig.S6. Plot of left-hand side of Eq. 3 against the reciprocal of the temperarure for CO adsorbed on H-[Al]-ZSM-5(50). (a) O−H stretching region (b) C−O stretching region. R linear regression coefficient; SD standard deviation.

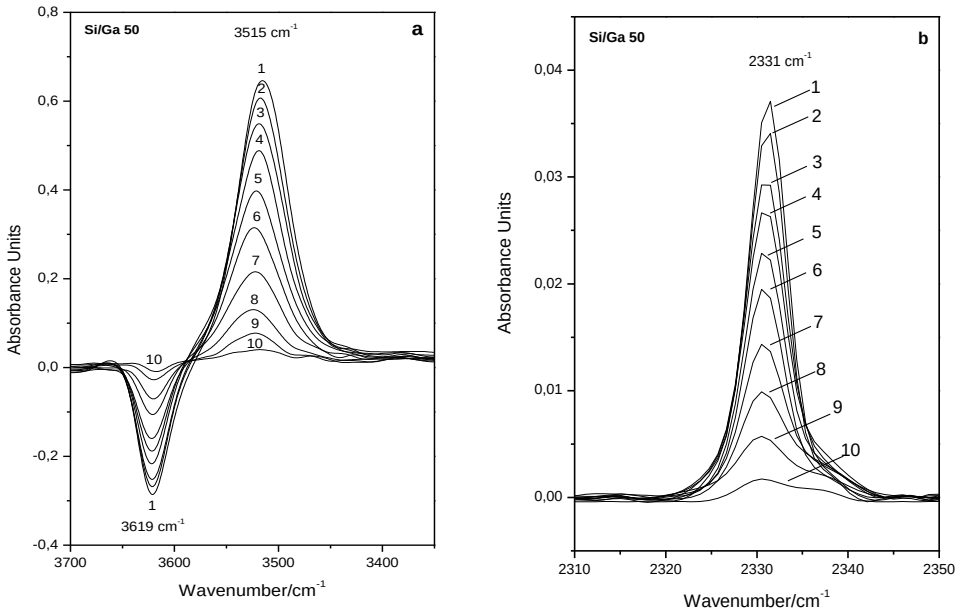

Fig.S7. (a) Representative variable-temperature IR spectra (O−H stretching region) of adsorbed N_2 on H-[Ga]-ZSM-5(50). The spectra are shown in the difference mode. (b) N−N stretching region. From 1 to 10, temperature goes from 123 to 162 K and equilibrium pressure from 1.4to 5.9 mbar.

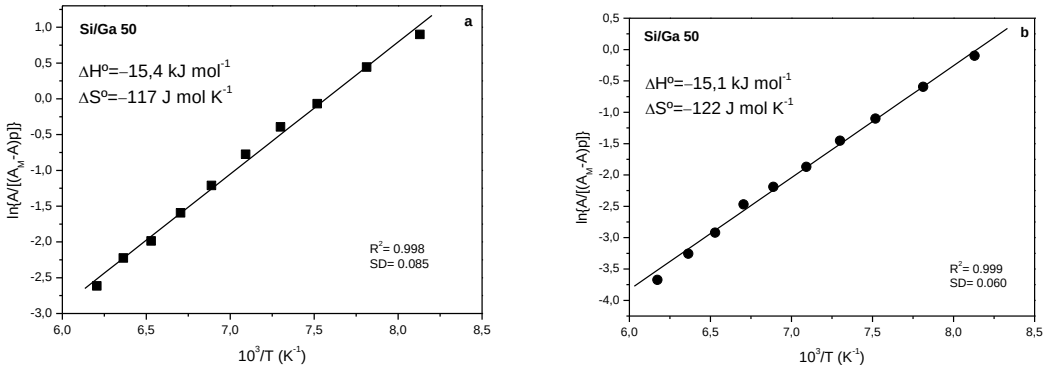

Fig.S8. Plot of left-hand side of Eq. 3 against the reciprocal of the temperarure for N_2 adsorbed on H-[Ga]-ZSM-5(50). (a) O−H stretching region (b) N−N stretching region. R linear regression coefficient; SD standard deviation.

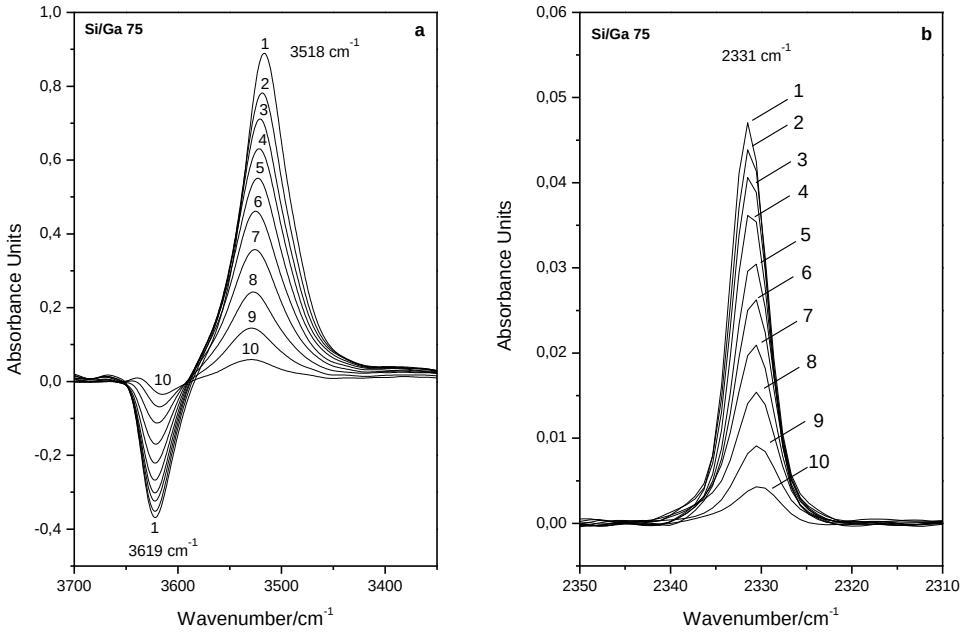

Fig.S9. (a) Representative variable-temperature IR spectra (O−H stretching region) of adsorbed N_2 on H-[Ga]-ZSM-5(75). The spectra are shown in the difference mode. (b) N−N stretching region. From 1 to 10, temperature goes from 113 to 159 K and equilibrium pressure from 0.36 to 6.19 mbar.

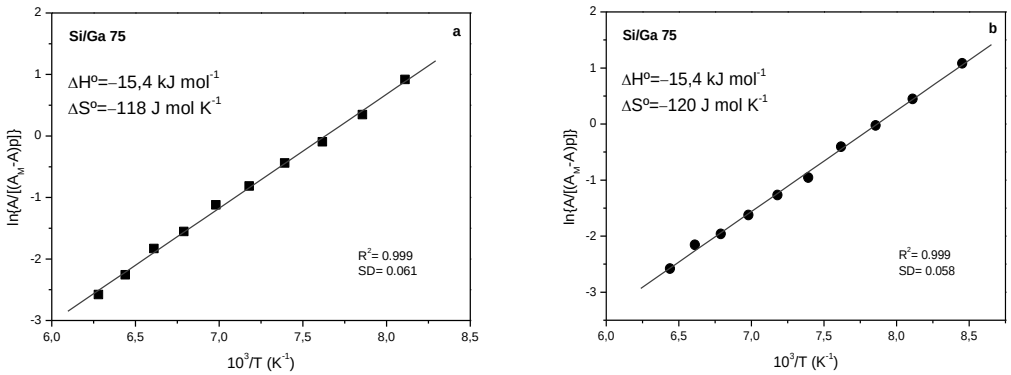

Fig.S10. Plot of left-hand side of Eq. 3 against the reciprocal of the temperarure for N_2 adsorbed on H-[Ga]-ZSM-5(75). (a) O−H stretching region (b) N−N stretching region. R linear regression coefficient; SD standard deviation.

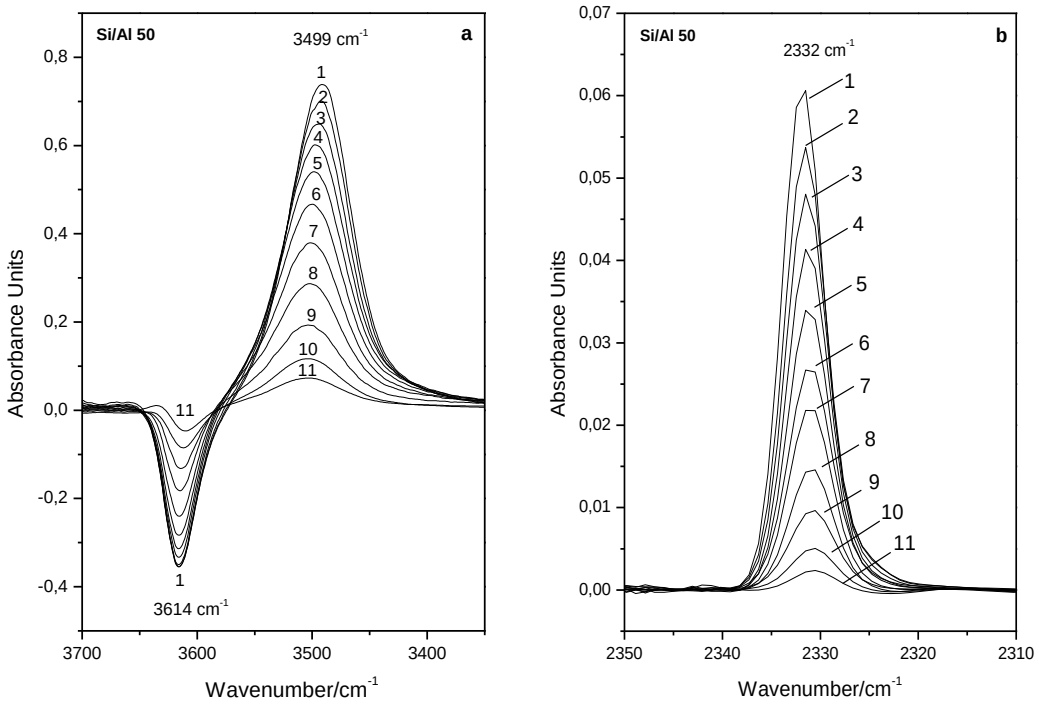

Fig.S11. (a) Representative variable-temperature IR spectra (O−H stretching region) of adsorbed N_2 on H-[Al]-ZSM-5(50). The spectra are shown in the difference mode. (b) N−N stretching region. From 1 to 11, temperature goes from 125 to 173 K and equilibrium pressure from 1.3 to 5.8 mbar.

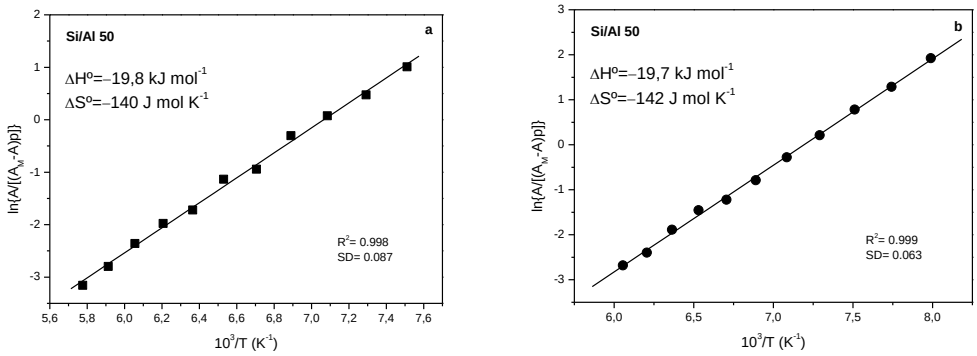

Fig.S12. Plot of left-hand side of Eq. 3 against the reciprocal of the temperarure for N_2 adsorbed on H-[Al]-ZSM-5(50). (a) O−H stretching region (b) N−N stretching region. R linear regression coefficient; SD standard deviation.